Received: 11 September 2025 | Revised: 8 December 2025 | Accepted: 13 December 2025

DOI: 10.1002/dvdy.70112

RESEARCH ARTICLE

Developmental Dynamics | AMERICAN ASSOCIATION FOR ANATOMY | WILEY

Oogenesis and germinal bed morphology of the brown anole (*A. sagrei*)

Bonnie K. Kircher[1] | **Antonia Weberling**[2,3,4,5] | **Erin J. Vance**[6] | **Natalia A. Shylo**[5,7] | **Katherine Starr**[8] | **Zoe B. Griffin**[1,6] | **Hannah Wilson**[5] | **Melainia McClain**[5] | **Florian Hollfelder**[4] | **Suzannah A. Williams**[3] | **Thomas J. Sanger**[8] | **Richard R. Behringer**[1] | **Paul A. Trainor**[5,9]

[1]Department of Genetics, University of Texas MD Anderson Cancer Center, Houston, Texas, USA

[2]All Souls College, University of Oxford, Oxford, UK

[3]Nuffield Department of Women's and Reproductive Health, University of Oxford, Oxford, UK

[4]Department of Biochemistry, University of Cambridge, Cambridge, UK

[5]Stowers Institute for Medical Research, Kansas City, Missouri, USA

[6]Department of Biosciences, Rice University, Houston, Texas, USA

[7]Department of Biological and Biomedical Sciences, Rowan University, Glassboro, New Jersey, USA

[8]Department of Biology, Loyola University Chicago, Chicago, Illinois, USA

[9]Department of Cell Biology and Physiology, University of Kansas Medical Center, Kansas City, Missouri, USA

Correspondence
Bonnie K. Kircher, Department of Genetics, University of Texas MD Anderson Cancer Center, Houston, TX, USA.
Email: bkkircher@mdanderson.org

Antonia Weberling, All Souls College, University of Oxford, Oxford, UK; Nuffield Department of Women's and Reproductive Health, University of Oxford, Oxford, UK; Department of Biochemistry, University of Cambridge, Cambridge, UK; Stowers Institute for Medical Research, Kansas City, Missouri, USA.
Email: antonia.weberling@all-souls.ox.ac.uk

Funding information
Stowers Institute for Medical Research, Grant/Award Number: 1008; European Research Council, Grant/Award Number: 695669; Isaac Newton Trust; National Science Foundation, Grant/Award

Abstract

Background: The brown anole is a model species of the genus *Anolis*, a squamate (encompassing lizards and snakes) group widely studied in evolutionary, behavioral, and developmental biology. Full genome annotation, the establishment of gene editing techniques, and comprehensive description of reproductive tract morphology and embryogenesis in this species have laid the foundation for functional studies. However, analysis of brown anole oogenesis is still required and vital to optimize genome modification, mutant line establishment, and analyses of the evolution of reproductive developmental mechanisms.

Results: Here, we characterize ovary morphology and gametogenesis in the female brown anole, *Anolis sagrei,* using brightfield imaging, microCT, histology staining, electron microscopy, and confocal imaging. We define 10 stages of oocyte maturation, which commences inside the oogonial nest within the germinal bed and concludes with the mature follicle ready to ovulate based on follicle size, yolk acquisition, and follicular, cellular, and basement membrane architecture.

Bonnie K. Kircher and Antonia Weberling contributed equally to this study.

Numbers: 1942250, 2209150; National Institutes of Health, Grant/Award Numbers: 5R01HD113569, CA16672, HD114881, HD30284, T32HD098068; University of Texas MD Anderson Cancer Center; All Souls College, University of Oxford; Engineering and Physical Sciences Research Council, Grant/Award Number: EP/Y032756/1

Conclusions: We describe the complete oogenesis of the brown anole in 10 stages and report that oogenesis is highly conserved within iguanians, a suborder of lizards. With our staging framework, we lay the foundation for functional studies of oogenesis and optimized gene-editing.

KEYWORDS

brown anole, follicle development, germinal bed, oocyte, oogenesis, ovary, reptiles, squamates

1 | INTRODUCTION

Non-avian reptiles exhibit striking divergence from mammals and birds in their manner of oogenesis. In mammals and birds, oocyte development occurs during embryogenesis, pauses during meiosis I, and resumes at sexual maturity. This results in most mammals and birds containing a finite number of oocytes in their ovaries[1,2] in contrast to non-avian reptiles (lizards, snakes, crocodilians, and turtles).[3] Ovaries of lizards and snakes generate oocytes continuously from the so-called germinal bed, located at the dorsal surface of the ovary.[4] There, the stem cells within the oogonial nest produce primordial follicles. During this process, the oogonial stem cells transition seasonally from mitosis to meiosis, such that the stem cells in the germinal bed are mitotic while the primordial follicles transition to meiosis.[5] Not all lizards have a single germinal bed; some species can have up to two germinal beds per ovary, and each germinal bed may ovulate over 200 times per ovulatory period.[6] However, despite some detailed histological studies of the reptilian ovary, including those in lizards,[3,7–16] the techniques were limited to histology and ultrastructure electron microscopy across relatively few follicular stages, making comprehensive understanding of germinal bed diversity and oocyte maturation poorly understood.

In non-avian reptiles, the stages of ovarian follicle development have been described with general conservation observed between species. In short, immature follicles exit the germinal bed and are surrounded by a single layer of pre-follicular cells. As the oocyte matures, the follicle enlarges while the pre-follicular cells mature into granulosa-like cells that surround the maturing follicle.[17] In mammals, steroidogenic granulosa cells communicate with the oocyte on one side and with the differently steroidogenic theca cells on the other side.[18] In the non-avian reptile ovary, the granulosa-like cells are also covered by theca cells.[19] As follicle development progresses, enlarged cells emerge in the granulosa cell layer including "intermediate" and "pyriform" granulosa cells. A layer of small granulosa cells lies directly over the oocyte while the enlarged intermediate and pyriform granulosa cells sit on top of the small granulosa cells, toward the outside of the follicle.[19] With the emergence of these cell types, the granulosa cell layer thickens. During more mature stages of follicular development, the follicular epithelium thins, and these enlarged pyriform cells establish intracellular bridges between the follicular epithelium and the oocyte.[10] Although the pyriform granulosa cells are characteristic of vitellogenic follicles,[7] their precise function remains unknown. At the latest, most mature stages of folliculogenesis, the epithelium becomes thinner until the mature vitellogenic pre-ovulatory follicle is only surrounded by a single cell layer.[20]

The brown anole (*Anolis sagrei*) has emerged as a representative species of the genus *Anolis* over the last two decades. *Anolis* comprises over 400 species that are distributed across the Caribbean, Middle and South America. Given the growing number of experimental and genomic tools, *Anolis* has become a primary model for the study of evolution, ecology, behavior, and physiology.[21] *Anolis* also serves as an important outgroup for genomic and developmental comparisons among birds, non-avian reptiles, and mammals.[22–25] Numerous tools have laid the basis for functional studies in the brown anole, most notably a high-quality annotated genome,[26] the establishment of CRISPR/Cas9 gene edited knockouts[27] and the generation of immortalized fibroblast lines.[28] However, CRISPR-Cas9 genome editing requires injection of pre-ovulatory follicles and currently has a success rate of only 10%–15%.[27] A better understanding of reproductive and developmental progression is needed to increase the efficiency of these techniques and for further functional studies.

The morphology of the reproductive tract and embryogenesis have been described for the brown anole.[29–31] Brown anole females have a duplex reproductive tract with uteri that coalesce at the cloaca.[29] Ovulation occurs every 5–10 days, alternating between the right and the left ovary,[32,33] resulting in about one egg being laid per week during the breeding season from May to September.

Oogenesis has previously been studied in two iguanian genera. In *Anolis pulchellus*, 4 stages of follicular maturation have been described[9] that loosely correlate

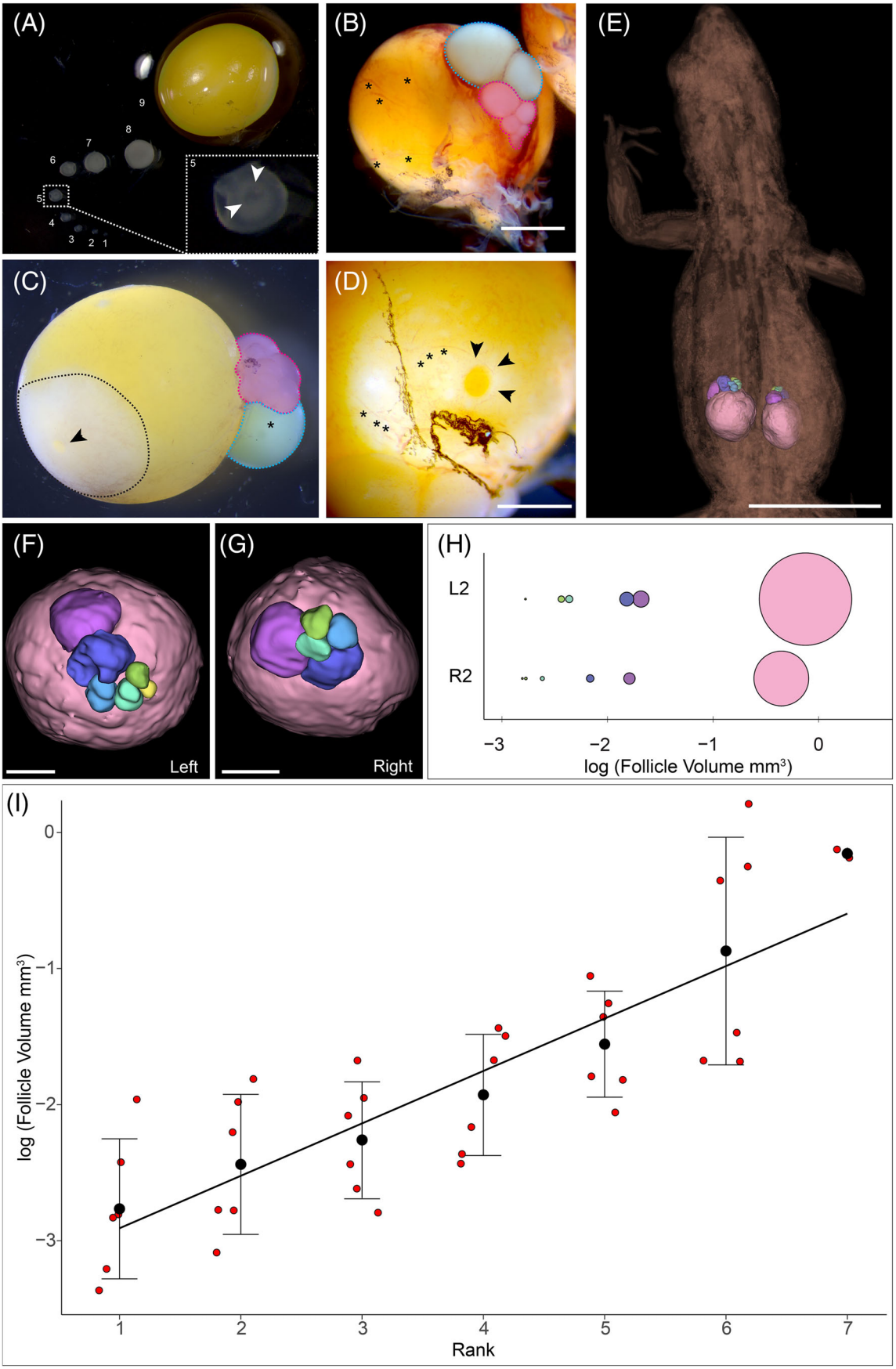

FIGURE 1 Legend on next page.

with the 9 more detailed stages defined for four *Tropidurus* species.[8] However, a detailed description of ovary and follicle development in the genus *Anolis* does not exist. To enable higher success rates for gene editing and inform functional studies, we need to better understand ovarian follicular morphology, development, and maturation.

Here, we provide a detailed description of *Anolis sagrei* oogenesis and ovarian morphology using brightfield imaging, computed tomography (CT) scans, scanning transmission electron microscopy (STEM), and histology staining, as well as confocal imaging. Guided by the description of follicle development in 9 stages in *Tropidurus*,[8] we define 10 consecutive stages of oogenesis in the brown anole, including one novel stage preceding the stages described in *Tropidurus*. We analyze follicle development through assessment of overall follicle size, the width and architecture of the follicular epithelium, and basement membrane composition. Taken together, our work lays the foundation for functional studies of non-avian reptile oogenesis and optimized CRISPR/Cas9 genome editing.

2 | RESULTS

2.1 | Brightfield and volumetric analysis of ovarian follicle growth

The ovary of the brown anole is composed of follicles that vary significantly in size and color (Figure 1A–C). The smallest follicles are colorless, then they become white and eventually beige due to yolk acquisition while increasing in size. These immature follicles are found in varying numbers in every ovary. In addition to these follicles, each ovary contains a maximum of one mature, yellow yolk-filled follicle, which is much larger than the beige follicles. It exhibits a bright yellow color and is enveloped by a vascularized, thin tissue (Figure 1B/D, asterisks). The germinal vesicle can be observed in every follicle (Figure 1A, higher magnification) but becomes more apparent upon the initiation of vitellogenesis (Figure 1C asterisk). In mature follicles, the germinal vesicle is found in the center of a white plate, the germinal disk (Figure 1C, dashed lines, Figure 1C/D, arrows). To quantify the dramatic size increase between immature, maturing, and the mature follicle and to understand whether these characteristic size differences were also present in situ, we assessed the volume of ovarian follicles following microCT imaging of whole females (Figure 1E). The ovaries are located dorsally in the coelomic cavity of the lizard, just anterior to the cloaca (Figure 1E). We digitally segmented the follicles on both the left and right ovaries (Figure 1F/G, raw data Figure 2A/B,D/E), where we observed the increase in size between the immature (yellow/cyan/green highlight) and the mature follicles (pink highlight) (Figure 1F/G, raw data Figure 2A/B,D/E). Plotting the follicle volume, we hypothesized that ovarian follicle size increases exponentially (Figure 1H, raw data Figure 2C,F). Following quantitative analysis of left and right ovaries of three females, we confirmed an exponential increase in follicle volume occurred during oogenesis (Figure 1I, Table 1). This trend also holds true when analyzing follicle volume across all three biological replicates at once (Figure 1I; $p = 6.656e\text{-}10$, $R2 = 0.6483$, $F[1,36] = 69.2$). We did not observe significant differences between left and right ovaries and therefore the data were pooled for further analysis (individual statistics in Table 1). Taken together, our volumetric analysis of different-aged follicles in anole ovaries revealed an exponential volume increase during maturation.

2.2 | Follicle maturation is accompanied by changes in yolk density patterns

Following our brightfield microscopy assessment that suggested progressive yolk acquisition upon follicle maturation, we collected cross-sections of whole ovaries and individual germinal vesicles and analyzed them using hematoxylin and eosin (H&E) staining (Figure 3, raw data Figure 4). H&E staining of whole ovary sections revealed distinct density patterns within the yolk of different sized follicles (Figure 3A–E). Mature vitellogenic

FIGURE 1 Volumetric analysis of the brown anole ovary. (A)–(D) Brightfield images of anole ovaries. (A) 9 follicles dissected from a single ovary with (1) as smallest and (9) as largest. Higher magnification of follicle (5), white arrows indicate the germinal vesicle. Ovary morphology (B/C) early follicles (magenta highlight), initiation of yolk acquisition (cyan highlight), (B) asterisks blood vessels, scale bar = 2 mm. (C) Asterisk in cyan highlighted follicle germinal vesicle. Dashed outline: Germinal disk, arrow: germinal vesicle. (D) Higher magnification of the germinal disk. Asterisks: Blood vessels. Arrows highlight the germinal vesicle, scale bar = 1 mm. (E)–(G) CT scans of ovaries from fixed anole females. Body visible in brown. Individual follicles segmented and color-coded. (E) Position of ovaries within the abdomen, scale bar = 10 mm. (F) Higher magnification of the left ovary, scale bar = 1 mm. (G) Higher magnification of the right ovary, scale bar = 1 mm. (H) Volumetric analysis of follicle size in left and right ovaries. Logarithmic scale. (I) Quantitative analysis of follicle volumes of six ovaries. Scatter plot mean ± StDev. Rank is assigned based on follicle size so that the smaller follicles have a lower rank.

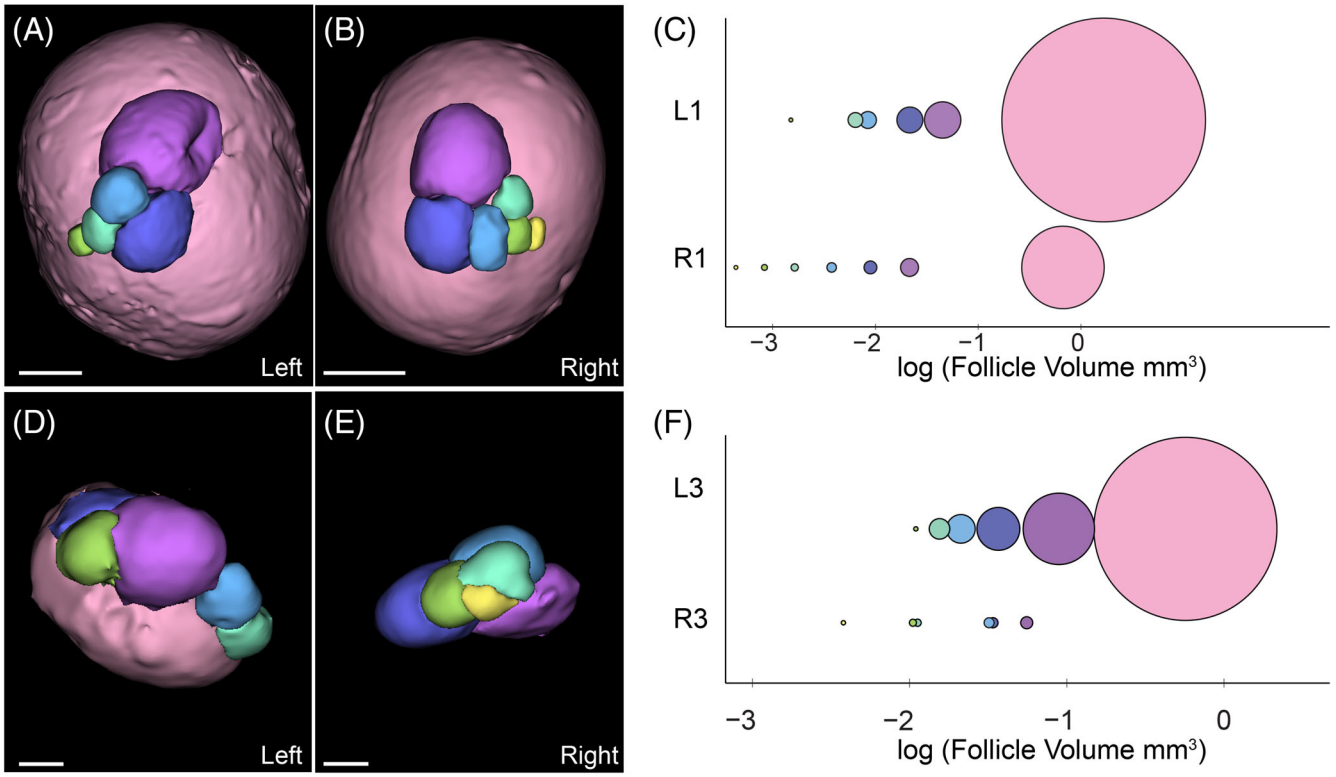

FIGURE 2 Additional biological replicates of CT scan segmentation of brown anole ovaries. (A/B) CT scan segmentations of ovaries from fixed anole females. Individual follicles segmented and color-coded. Replicate 2 (Anole 1) left ovary (A) and right ovary (B), scale bar = 1 mm. Replicate 3 (Anole 3) left ovary (D) and right ovary (E), scale bar = 1 mm. C,F. Volumetric analysis of follicle size in left and right ovaries.

TABLE 1 Regression statistics for follicular volume across six individual ovaries analyzed.

Anole	Ovary	*p*-value	*F* (1,3)	*R*-squared
1	L	.002884	81.22	0.9525
1	R	.0001403	625.2	0.9936
2	L	.003535	70.62	0.9457
2	R	.01361	27.34	0.8682
3	L	.004972	55.77	0.9319
3	R	.003753	67.76	0.9435

(mv) follicles are composed of homogenous, dense yolk that has a grainy appearance (Figure 3A, arrows, Figure 3B/B′) surrounded by a thin cell monolayer (Figure 3B arrows). Maturing vitellogenic follicles exhibit three distinct layers of yolk (Figure 3C/C′/C″). The outermost layer 1 is dense and rich in lipid droplets (Figure 3C′, arrows). These characteristics are in stark contrast to layer 2, which appears spongy with a low density, and fills most of the follicle volume (Figure 3C/C′/C″ 2). In the middle of the follicle, a small third layer is present which again exhibits higher density, but no large lipid droplets as observed in layer 1 (Figure 3C/C″ 3). Early vitellogenic (ev) follicles are composed of 2 different layers (Figure 3D/D′/D″). The outer layer, which constitutes most of the follicle, is dense and homogenous (Figure 3D/D′ 1). The inner layer appears loose and spongy, like layer 2 in the maturing vitellogenic follicle (Figure 3D/D″). In pre-vitellogenic (pv) follicles (Figure 3E), the yolk/cytoplasm has a homogenous structure and only exhibits small foci of high density surrounded by lower density (Figure 3E′, asterisks). Interestingly, we observed a set of structures inside the germinal vesicle that may be condensed DNA (Figure 3E″, arrows). To understand these qualitative observations in more detail, we measured yolk density by quantifying the changes in gray-value across the histological sections of the four stages of yolk development using plot profiles (Figure 3F, raw data Figure 4A–E). Gray values are higher and more consistent in pv follicles correlating with the homogeneous structure of the yolk/cytoplasm (Figure 3F, raw data Figure 4A–E). In ev follicles, the gray values are higher in the middle of the follicle compared to the outer edges of the follicle, correlating with the layered morphology of the yolk developing at these stages (Figure 3F, raw data Figure 4A–E). In mv follicles, gray values are variable across the plot profile,

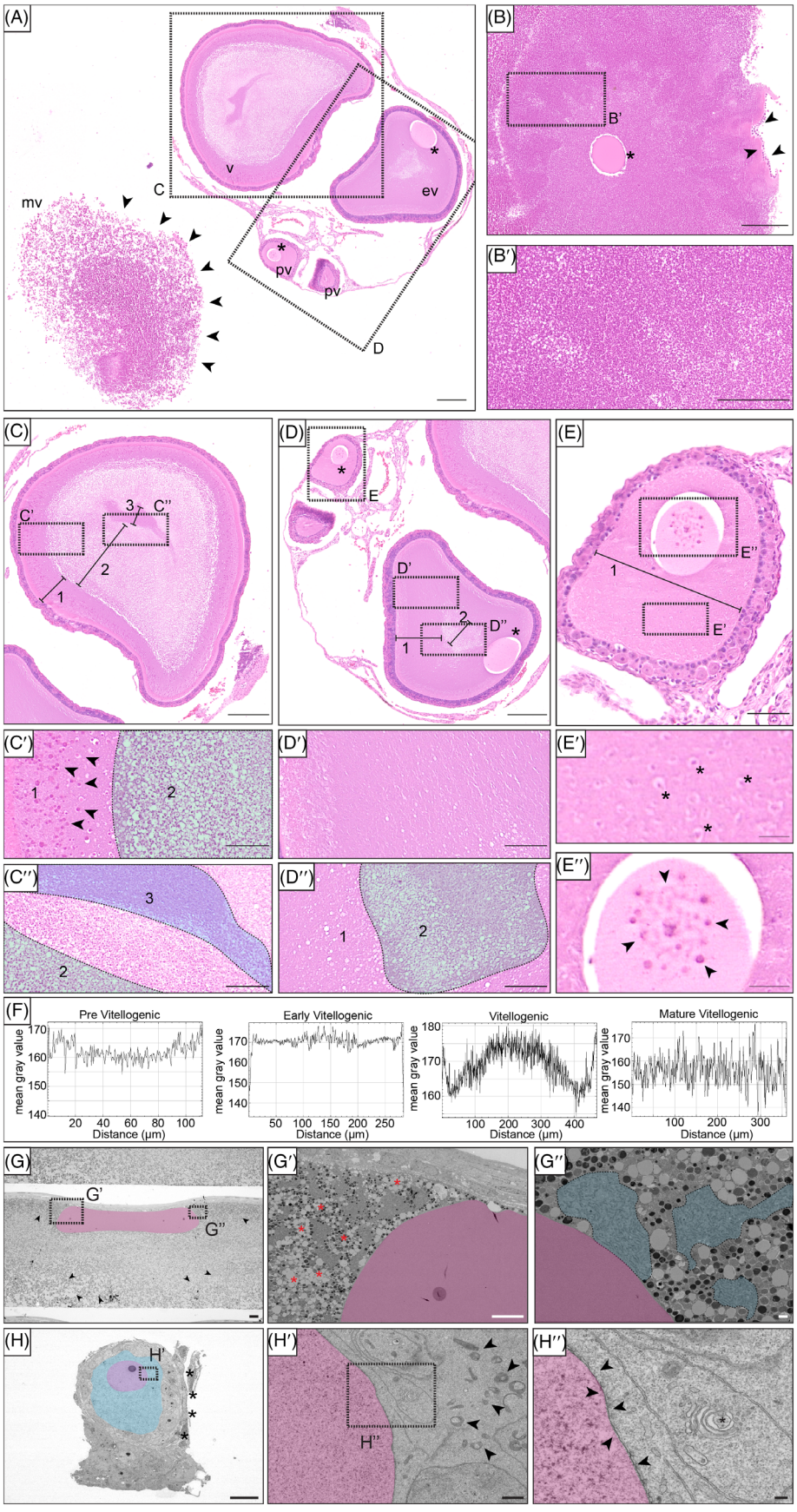

FIGURE 3 Legend on next page.

reflecting the homogeneous lipid droplet architecture in the cytoplasm of these follicles.

To gain higher resolution insight into the substructure of the yolk in vitellogenic (v) versus pv follicles, we performed STEM (Figure 3G/H, raw data Figure 4F/G). The yolk of vitellogenic follicles is rich in lipid droplets (Figure 3G arrows, Figure 3G′, asterisks, raw data Figure 4F) and exhibits high numbers of tightly packed mitochondria (blue highlight) in direct proximity to the germinal vesicle (magenta highlight) (Figure 3G″, raw data Figure 4F″). In contrast, pv follicles do not contain lipid droplets in their cytoplasm (Figure 3H, blue highlight, raw data Figure 4G). Mitochondria can be observed but at much lower density than in vitellogenic follicles (Figure 3H′, arrows, raw data Figure 4G′) and are not found in direct proximity to the germinal vesicle (Figure 3H″, raw data Figure 4G″). Instead, elongated Endoplasmic Reticulum and Golgi apparatus (asterisk) were observed surrounding the germinal vesicle (Figure 3H″, raw data Figure 4G″). Interestingly, we identified the germinal bed in direct proximity to the pv follicle (Figure 3H asterisks, raw data Figure 4G).

2.3 | The different stages of oogenesis can be distinguished through the changes in the follicular epithelium

Following our observation of the germinal bed (Figure 3H, raw data Figure 4G), we examined the progression of ovarian follicle development and maturation from oogonia to a mature vitellogenic follicle. Therefore, we carried out H&E staining of cross-sections of ovaries (Figure 5A–C, raw data Figure 6). In the germinal bed, we observed oogonia and primordial follicles (Figure 5A,D1, raw data Figure 6D1). Upon initiation of follicle development, we observed distinct differences in the follicular epithelium. Across all follicle stages, epithelium thickness ranged from a single cell layer in the earliest stages (Figure 5A blue highlight) to a thick, multilayered envelope of different cell types in the later stage follicles (Figure 5B). The mature vitellogenic follicle exhibits again only a single cell layer (Figure 5C). We then analyzed follicle morphology and composition of the follicular epithelium (Figure 5D, raw data Figure 6D). In the germinal bed, two distinct populations of germ cells can be observed. Numerous oogonia cluster into the oogonial nest (Figure 5D1, blue highlight, raw data Figure 6D1). The individual oogonia are characterized by small, dense nuclei and cytoplasm devoid of eosin staining. The nuclei are not round but rather exhibit signs of mitosis, such as aligned or condensed chromosomes (raw data Figure 6D1i). We term this stage Ia. The second population we could define in the germinal bed are primordial follicles (Figure 5D1, yellow highlight, raw data Figure 6D1ii). Here, the nuclei are no longer condensed but round and of lighter staining. The diameter of these cells has enlarged by a factor of two-three compared to the oogonia, and the cytoplasm is positive for eosin. These primordial follicles are not as tightly packed as the cells in the oogonial nest. Instead, they

FIGURE 3 Analysis of yolk composition during vitellogenesis. (A) H&E staining of ovary cross section. The ovary contains a vitellogenic follicle (mv). A maturing vitellogenic follicle (v), an early vitellogenic follicle (ev), and several previtellogenic follicles (pv). Arrows indicate the mature vitellogenic follicle that broke apart during processing; box C indicates the higher magnification of (C); box D indicates higher magnification of (D); scale bar = 200 μm. (B) H&E staining of mature vitellogenic follicle. Asterisk indicates germinal vesicle; arrows indicate cell layer surrounding follicle. Box B′ outlines higher magnification of (B′); scale bar 200 μm. (B′) higher magnification of yolk in mature vitellogenic follicle. Yolk dense and homogenous; scale bar = 100 μm. (C) H&E staining of maturing vitellogenic follicle. Yolk exhibits 3 (1–3) distinct layers of different density and composition; scale bar = 200 μm. (C′) Higher magnification of layer 1&2. Layer 1 exhibits large darker droplets (arrows). Layer 2 (green highlight) is less dense; scale bar = 50 μm. (C″) Higher magnification of layers 2 (green) and 3 (cyan), which is denser than 2; scale bar = 50 μm. (D) Early vitellogenic follicle. Yolk is composed of 2 layers (1–2); boxes D′/D″ indicate higher magnifications. Asterisks indicate germinal vesicles. Box E indicates higher magnification of (E); scale bar = 200 μm. (D′) Homogenous yolk composition in layer 1; scale bar = 50 μm. (D″) Yolk composition of layer 1 versus layer 2 (green highlight); scale bar = 50 μm. (E) Pre-vitellogenic follicle. Yolk is homogenous (1). Boxes indicate higher magnifications; scale bar 50 μm. (E′) Yolk composition of pre-vitellogenic follicle. Asterisks indicate small foci of less density; scale bar = 10 μm. (E″) Germinal vesicle exhibits dense foci (arrows) that could be DNA, scale bar= 20 μm. (F) Plot profiles of yolk composition of pre-vitellogenic, early vitellogenic, vitellogenic and mature vitellogenic follicles. (G) STEM of mature vitellogenic follicle. Germinal vesicle highlighted in magenta. Yolk is filled with droplets (arrows). Boxes indicate higher magnifications (G′/G″). scale bar = 20 μm. (G′) The yolk is filled with lipid droplets (asterisks); scale bar = 10 μm. (G″) High concentrations of mitochondria are observed (blue highlight); scale bar = 1 μm. (H) STEM of previtellogenic follicle. Germinal vesicle highlighted in magenta. Cytoplasm/yolk (blue highlight) lacks lipid droplets and the punctae-like structure found in (G); box indicates higher magnification (H′). Asterisks indicate germinal bed; scale bar = 20 μm. (H′) Cytoplasm/yolk exhibits low density of mitochondria and no lipid droplets; scale bar = 1 μm. (H″) Double membrane (arrows) surrounding the germinal vesicle not in direct proximity of lipid droplets or mitochondria; asterisk indicates Golgi apparatus; scale bar = 200 nm.

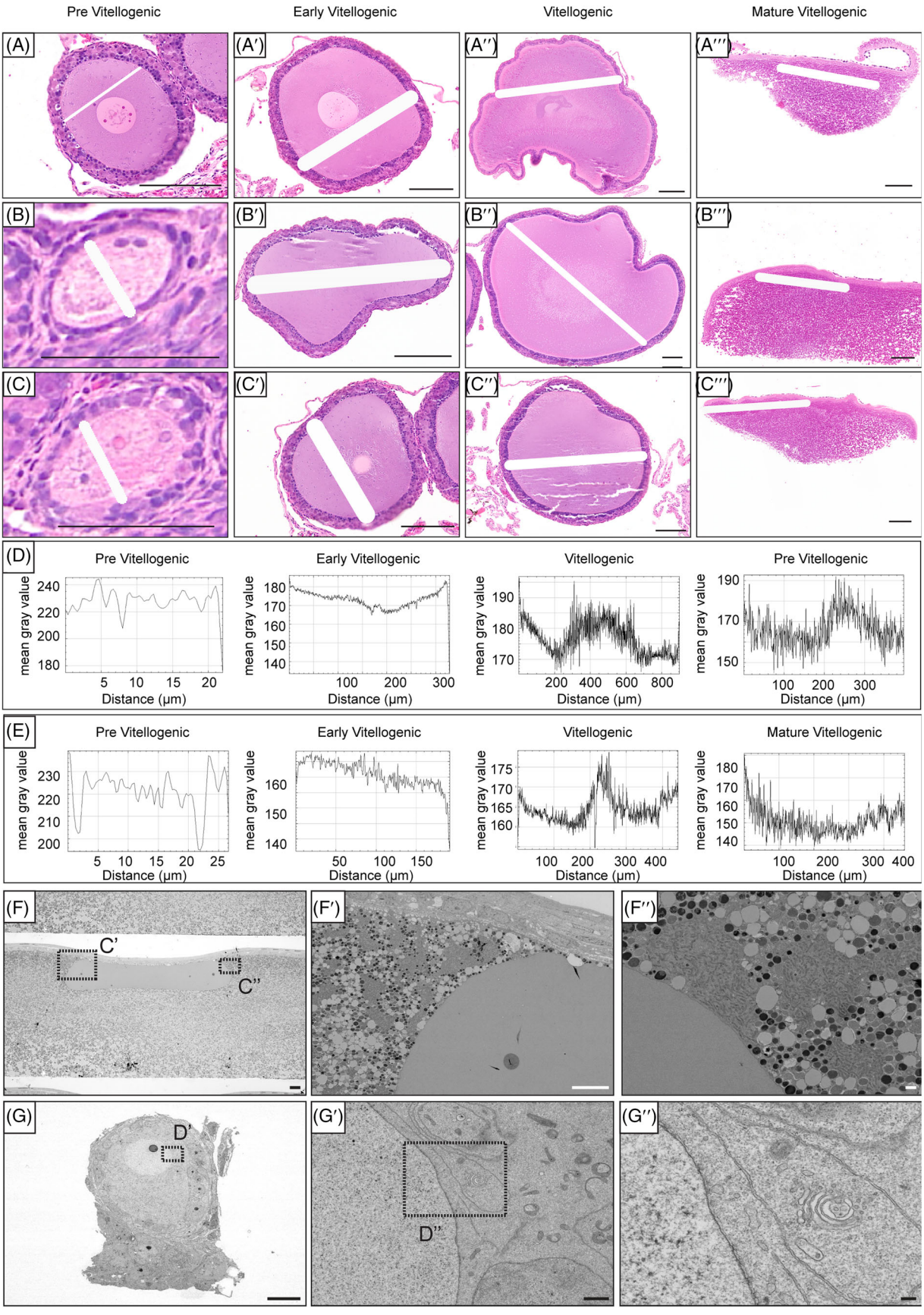

FIGURE 4 Legend on next page.

appear interspersed with epithelial cells. We termed this stage Ib.

At the next stage (stage II), the follicle size increases further and is enveloped by a tightly packed layer of granulosa cells surrounding the oocyte (Figure 5D2, raw data Figure 6D2). The granulosa cells exhibit characteristic rounded nuclei (asterisks). We also observed the first theca cells surrounding the granulosa cells defined by their elongated nuclear shapes (arrows).

At stage III (Figures 5D3, raw data Figure 6A, 6D3), the follicle has a diameter of 42.3 mm (Table 2). The first pyriform granulosa cells (Figure 5D3, yellow highlight) appear in a multilayered granulosa layer that does not exhibit clear organization of the different cell types. The theca cells (Figure 5D3, arrows) have formed a double to triple layer on top of the granulosa cells.

At stage IV, as the follicle continues to enlarge (Figure 5D4, raw data Figure 6B,D4), the number of pyriform granulosa cells (yellow highlight) increases while the intermediate and small granulosa cells are localized closer to the follicle (asterisks). The theca cells continue to be arranged in a minimum of three layers (Figure 5D4, arrows).

At stage V (Figure 5D5, raw data Figure 6D5), the granulosa cell layer has matured into multiple layers of small and intermediate granulosa cells close to the follicle (Figure 5D5, asterisks), while the pyriform granulosa cells (yellow highlight) form a mono- to double layer on top of the small and intermediate cells (asterisks). The theca cells have increased to 6–7 layers (arrows).

At stage VI, the follicle has initiated vitellogenesis (Figure 5B ev, raw data Figure 6D6), and the pyriform granulosa cells no longer form a continuous layer (Figure 5D6, yellow highlight). The remaining granulosa cell layer is composed almost exclusively of intermediate cells (asterisks), with very few remaining small granulosa cells.

At stage VII, the granulosa cell layer has significantly thinned, decreasing from ~5 to 2–3 cell layers (Figure 5D7, raw data Figure 6D7). Pyriform granulosa cells contact the oocyte (yellow highlight). As no small and only a few intermediate granulosa cells can be observed, most of the granulosa layer is populated by large granulosa cells. The theca cell layer remains unchanged at this stage.

At stage VIII, the granulosa cell layer has thinned to 1–2 cell layers (Figure 5D8, raw data Figure 6C,D8). All pyriform granulosa cells (yellow highlight) are now in direct contact with the oocyte and have adopted a squamous shape. The theca cell layer remains unchanged, which results in about 50% of the follicle lining being composed of theca cells.

The mature follicle at stage IX has lost the granulosa cell layer and is covered by a thin cell layer that surrounds the entire follicle (Figure 5D9, raw data Figure 6D9).

We quantified changes in the follicular epithelium width across the different follicle stages described above. Upon the initiation of vitellogenesis, the width of the epithelium increases, but then, following an abrupt thinning of the follicular epithelium at stage VII, it returns to a single cell layer in mature, pre-ovulatory follicles (Figure 5E, Table 2). We then assessed follicle area across the different stages noting an increase as follicles mature (Figure 5F, Table 2). Finally, we measured changes in the cell composition of the granulosa layer by counting small and large (including both intermediate and pyriform) granulosa cells. We observed the population of large granulosa cells increase over time while the small granulosa cells gradually disappear (Figure 5G, Table 2).

2.4 | The subcellular structure of stage I–II and stage VIII follicles

Next, we focused on the subcellular structures at the initiation of stage II, and during later stage VIII, follicle development using STEM (Figure 7, raw data Figure 8). We therefore dissected individual follicles and studied the smallest follicle (Figure 7A, raw data Figure 8A). Following our stage descriptions (Figure 5D), we defined the follicle as stage II as it exhibits a single layer of granulosa cells, which have oval nuclei (blue highlight), and a thin layer of theca cells which present with highly elongated nuclei (green highlight) (Figure 7A′, raw data Figure 8A′). On the right-hand side of the follicle, we observed a group of cells with enlarged, more rounded nuclei and prominent nucleoli reminiscent of the structure of the germinal vesicle inside the follicle (Figure 7A″, raw data Figure 8A″). We hypothesize that

FIGURE 4 Additional biological replicates for analysis of yolk composition during follicle maturation. (A)–(C) Pictures of paraffin sections of ovarian follicles stained with H&E used for plot profile analysis. White line across section represents the selection from which the plot profile was generated. (A) Sections used for plot profile analysis in Figure 3F. (B) Sections used for plot profile analysis in Figure 4D. (C) Sections used for plot profile analysis in Figure 4E. (D)–(E) Additional biological replicates of plot profiles of mean gray value of yolk composition during follicle development. (F)–(G) STEM of pre-vitellogenic and mature vitellogenic follicle. Images from (F)–(G)/(H) without annotations and highlights. Scale bar for $C = 20$ µm, scale bar for $D = 200$ nm.

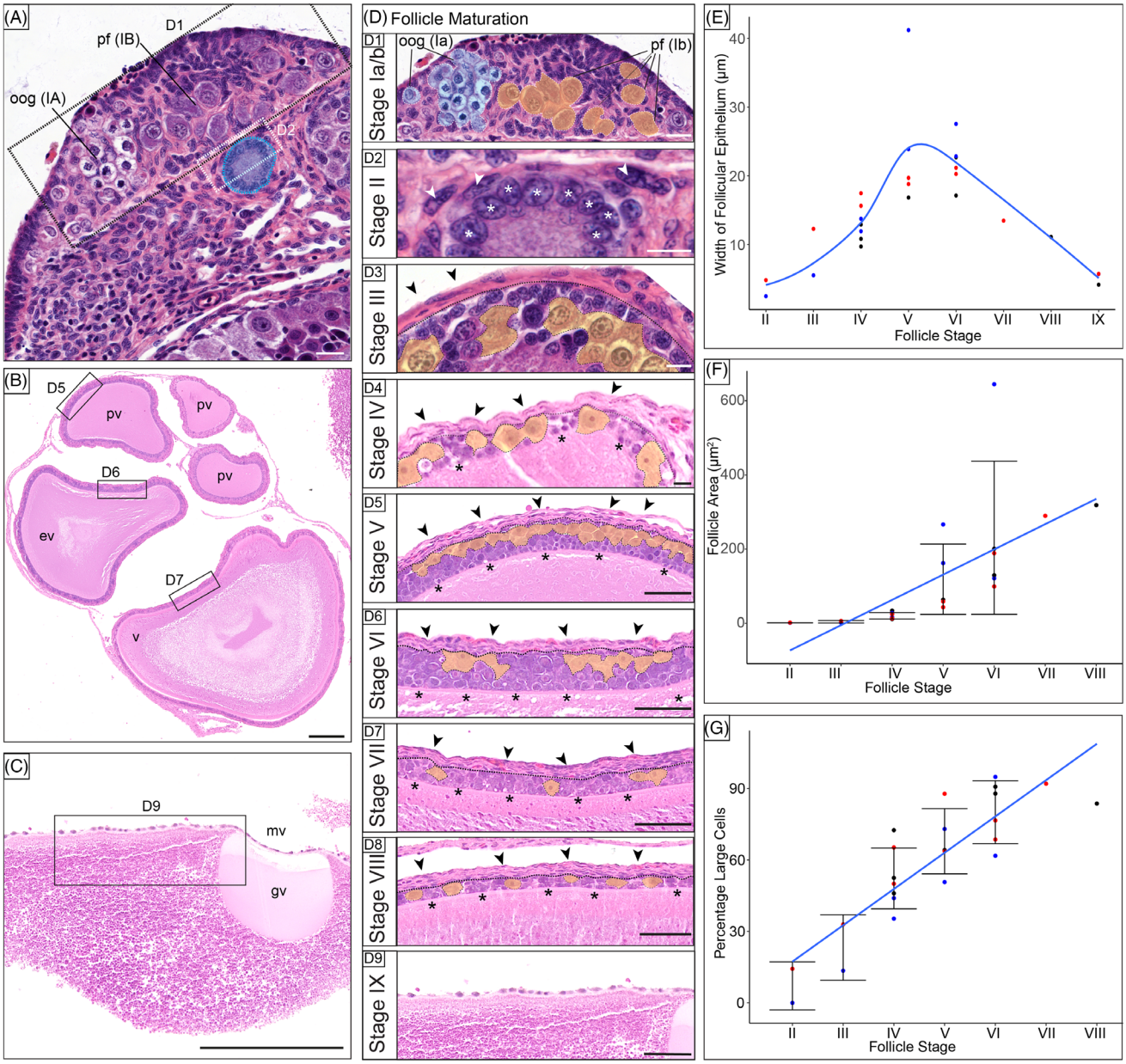

FIGURE 5 Histological analysis of germ cell maturation. (A) H&E stained ovarian cross section containing the germinal bed populated with oogonia (oog) and primordial follicles (pf), and a stage II follicle (blue highlight). Rectangles indicate higher magnification of Figure D1/D2 scale bar = 20 µm. (B) H&E stained ovarian cross section of previtellogenic to vitellogenic follicles. pv = previtellogenic, ev = early vitellogenic, v = vitellogenic. Rectangles indicate higher magnification of Figure D5–7. scale bar = 200 µm. (C) H&E stained cross section of mature vitellogenic follicle (mv). Germinal vesicle (gv) visible. Square indicates higher magnification of Figure D9 scale bar = 200 µm. (D) H&E staining of the 9 stages of follicle maturation (I–IX). (D1) oogonia (blue highlight, oog), primordial follicles (yellow highlight, pf), scale bar = 20 µm, (D2-9) granulosa cells (asterisks) and theca cells (arrows) are highlighted, (D2-4) scale bar = 10 µm, (D5-9) scale bar = 50 µm. (D4-8) dashed line between theca and granulosa cell layer, pyriform granulosa cells highlighted in yellow. All scale bars = 20 µm. (E) Quantitative analysis of the thickness of the follicular epithelium (granulosa and theca cells combined) from stage I–IX. (F) Quantitative analysis of follicle size from stage Ia-stage IX. (G) Quantitative analysis of the granulosa cell layer. The percentage of large (pyriform&intermediate) granulosa cells plotted over stages I–VIII. For (E)–(G), individual ovaries from lizards with ID numbers M121D (black data points), M127C (red data points), M122C (blue data points) were analyzed. Trendline is a linear model in *R*. Adjusted Statistical analysis: *R*-squared: 0.7605, *F*-statistic: 74.01 on 1 and 22 DF, *p*-value: 1.73e-08.

these are the oogonia based on their size[34] and our comparison to the oogonial nest described above (Figure 5D1). Beneath the follicle, we observed a group of 4 cells exhibiting markedly enlarged nuclei and cytoplasm (Figure 7A‴, raw data Figure 8A‴). We hypothesize that these cells are primordial follicles as they do not

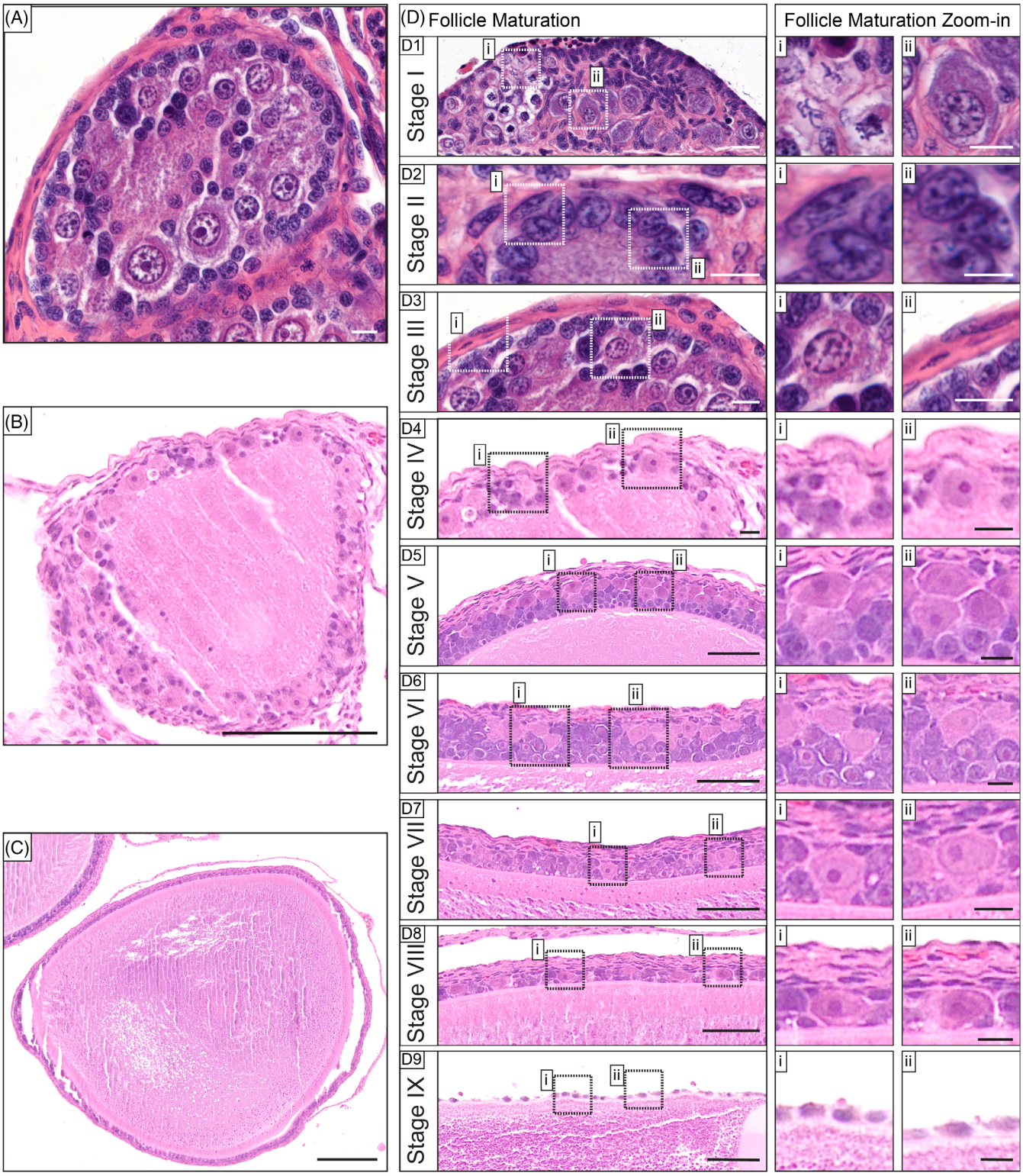

FIGURE 6 Raw data with no pseudo-coloring and higher magnification images of histology of the consecutive stages of oocyte maturation. (A) H&E staining of stage III follicle, higher magnification shown in Figure 3D3. Scale bar = 10 μm. (B) H&E staining of stage IV follicle, higher magnification shown in Figure 3D4. Scale bar = 100 μm. (C) H&E staining of stage VIII follicle, higher magnification shown in Figure 3D8. Scale bar = 200 μm. (D) H&E staining of the stages of anole follicle development, non-annotated copy of Figure 3D. higher magnifications illustrate different stage characteristics. (D2-4) scale bar = 10 μm, (D5-9) scale bar = 50 μm. (D1-2), i-ii scale bar = 5 μm, D3-9, i-ii scale bar = 10 μm.

TABLE 2 Measurements collected to quantify changes between ovarian follicle stages.

ID	Color	Yolk stage	Follicle number	Follicle stage	Small cell count	Large cell count	Total	Small%	Large%
M122C	Blue	pv	1	2	22	0	22	100	0
M127C	Red	pv	7	2	30	5	35	85.7142857	14.2857143
M122C	Blue	pv	2	3	32	5	37	86.4864865	13.5135135
M127C	Red	pv	6	3	55	27	82	67.0731707	32.9268293
M121D	Black	pv	2	4	58	64	122	47.5409836	52.4590164
M121D	Black	pv	4	4	88	75	163	53.9877301	46.0122699
M121D	Black	pv	3	4	60	158	218	27.5229358	72.4770642
M122C	Blue	pv	3	4	73	40	113	64.6017699	35.3982301
M122C	Blue	pv	4	4	79	62	141	56.0283688	43.9716312
M127C	Red	pv	5	4	85	85	170	50	50
M127C	Red	pv	8	4	66	124	190	34.7368421	65.2631579
M121D	Black	ev	6	5	171	306	477	35.8490566	64.1509434
M122C	Blue	pv	5	5	177	182	359	49.3036212	50.6963788
M122C	Blue	pv	7	5	139	375	514	27.0428016	72.9571984
M127C	Red	pv	9	5	35	252	287	12.195122	87.8048781
M127C	Red	ev	4	5	114	200	314	36.3057325	63.6942675
M121D	Black	ev	5	6	80	580	660	12.1212121	87.8787879
M121D	Black	ev	7	6	71	693	764	9.29319372	90.7068063
M122C	Blue	ev	6	6	109	176	285	38.245614	61.754386
M122C	Blue	v	8	6	30	548	578	5.19031142	94.8096886
M127C	Red	v	3	6	148	484	632	23.4177215	76.5822785
M127C	Red	ev	2	6	171	373	544	31.4338235	68.5661765
M127C	Red	v	1	7	54	617	671	8.04769002	91.95231
M121D	Black	V	1	8	103	529	632	16.2974684	83.7025317
M121D	Black	mv	8	9	N/A	N/A	N/A	N/A	N/A
M122C	Blue	mv	9	9	N/A	N/A	N/A	N/A	N/A
M127C	Red	mv	10	9	N/A	N/A	N/A	N/A	N/A

Follicle area µm	Follicle area µm	Follicle width 1	Follicle width 2	Follicle width 3	Average follicle width
1002.667	1.002667	2.828	1.795	3.145	2.47
1492	1.492	5.27	4.269	4.955	4.83133333
1730.444	1.730444	5.088	4.346	7.032	5.48866667
6282.667	6.282667	13	12.737	11.101	12.2793333
15193.22	15.19322	12.089	7.769	9.22	9.69266667
11097.889	11.097889	8.969	13.876	9.597	10.814
33913.778	33.913778	12.512	13.271	12.944	12.909
16314.778	16.314778	14.461	11.324	10.05	11.945
27410.111	27.410111	15.202	12.293	13.671	13.722
12911.778	12.911778	13.864	16.035	16.974	15.6243333
24580.222	24.580222	17.714	16.364	18.342	17.4733333
63410.899	63.410899	17.537	14.941	18.028	16.8353333
162134	162.134	18.487	24.413	28.674	23.858
266142.444	266.142444	32.77	42.165	48.671	41.202

TABLE 2 (Continued)

Follicle area µm	Follicle area µm	Follicle width 1	Follicle width 2	Follicle width 3	Average follicle width
43227	43.227	22.01	18.273	18.812	19.6983333
58554	58.554	15.563	21.715	19.128	18.802
200832	200.832	17.92	14.981	18.523	17.1413333
129527.667	129.527667	19.047	19.531	29.494	22.6906667
121226.444	121.226444	21.797	19.821	26.874	22.8306667
644370.889	644.370889	30.806	27.014	24.775	27.5316667
188771	188.771	22.103	20.276	21.095	21.158
99194	99.194	23.286	18.236	19.235	20.2523333
289749.333	289.749333	11.353	16.09	13.017	13.4866667
318553.222	318.553222	10.833	11.319	11.108	11.0866667
N/A	N/A	4.069	3.606	4.738	4.13766667
N/A	N/A	8.028	4.384	4.679	5.697
N/A	N/A	5.09	6.037	6.083	5.73666667

have organized granulosa cells around them but are interspersed with cells that may mature into the granulosa layer.

We then focused on a stage VIII follicle (Figure 7B/raw data Figure 8B) and observed a monolayer of granulosa cells overlaying the follicle (Figure 7B′/″, raw data Figure 8B′/″). The nuclei of these granulosa cells adopted a squamous shape (blue highlight), confirming our observations made with H&E staining (Figure 5). The theca cell nuclei are highly squamous (green highlight), and the theca cell layer is about two-thirds of the thickness of the follicular epithelium. Finally, we compared the subcellular architecture of the cytoplasm/yolk of stage II/stage VIII follicles and found that at stage II, the cytoplasm is populated by organelles such as Endoplasmic Reticulum and mitochondria, while the yolk of the stage VIII follicle is filled with lipid droplets (Figure 7A/raw data Figure 8A, Figures 7B″′, 8A Figure 8B″′). Our results detailed and confirmed characteristic changes in the follicular epithelium upon follicle maturation.

2.5 | Basement membrane architecture during follicle development

To investigate changes in basement membrane composition and thickness during follicle maturation, we performed trichrome staining on cross sections of ovaries (Figure 9A–E). The germinal bed was separated from maturing follicles by a thick layer of basement membrane (Figure 9A/A′, asterisks). Upon initiation of follicle development, the follicles appear enveloped in a thick layer of basement membrane (Figure 9A′, arrows). In stage III follicles (Figure 9A″), we observed a very thin basement membrane layer around the oocyte (asterisks) and a thick layer of basement membrane in the theca cell layer (arrows).

Once the granulosa and theca layers are fully established at stage V, two layers of basement membrane can be detected (Figure 9B), with one thin layer directly overlaying the maturing follicle (asterisks), while the other basement membrane is located at the granulosa-theca interface and is much thicker (arrows) (Figure 5B′). This double membrane on either side of the granulosa cell layer is retained throughout follicle maturation (Figure 9C/C′/D/D′). At stage IX, when the multiple cell layers are lost (Figure 9E), only the thin basement membrane layer directly overlying the oocyte remains (Figure 9E′/E″).

To investigate basement membrane localization in 3D, we performed whole-mount confocal imaging of ovaries containing stage I–VIII follicles, stained with Wheat Germ Agglutinin (WGA, a lectin that binds carbohydrate chains abundant in basement membranes). The germinal bed was localized based on its position and morphology (Figure 9F z85/z100), and the primordial follicles were identified as small pockets in tightly packed nuclei containing one slightly enlarged nucleus (Figure 9F z85 DAPI). Interestingly, these individual primordial follicles could also be distinguished with WGA staining, which formed distinct pockets around each oogonial cell (Figure 9F z85 WGA). The germinal bed appears separate from the follicles undergoing maturation (Figure 9F z100/z110, dashed line). At stage II (Figure 9F z110, higher magnification, asterisks), two basement membranes can be observed on either side of the granulosa

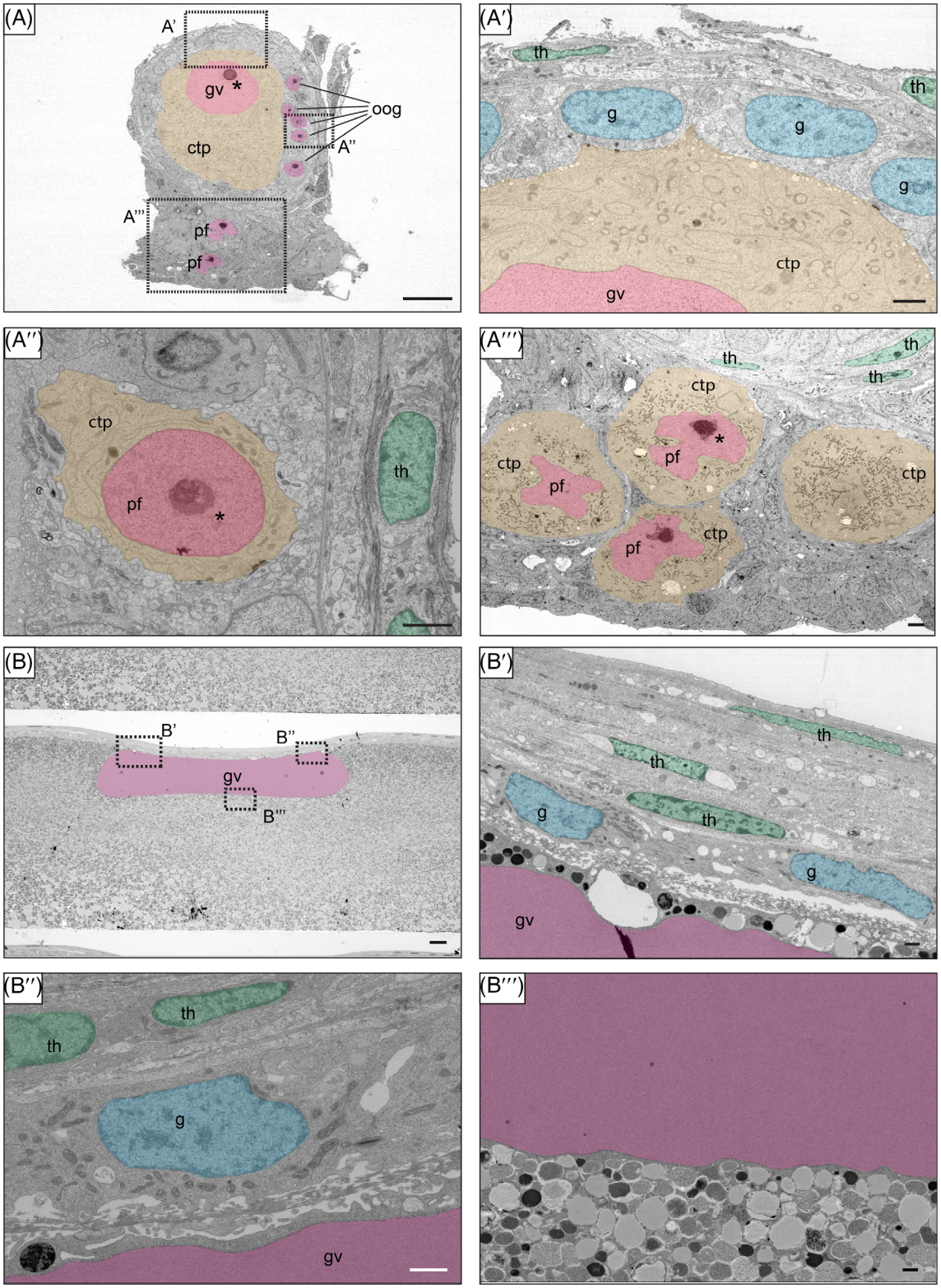

FIGURE 7 Subcellular architecture of the germinal bed A/B. STEM of germinal bed and stage II follicle (A) and stage VIII follicle (B), re-analysis of Data shown in Figure 3H. Squares indicate regions for higher magnifications. Color code: Germinal vesicle/germ cell nuclei (magenta highlight), cytoplasm of primordial/previtellogenic follicles (yellow highlight) granulosa cell nuclei (blue highlight), theca cell nuclei (green highlight), asterisks indicate nucleoli. ctp = cytoplasm, g = granulosa cell, gv = germinal vesicle, oog = oogonia, pf = primordial follicle, th = theca cell. Scale bars: (A/B) = 20 μm. (A′)-(A″′) = 2 μm, (B′)–(B″′) = 1 μm.

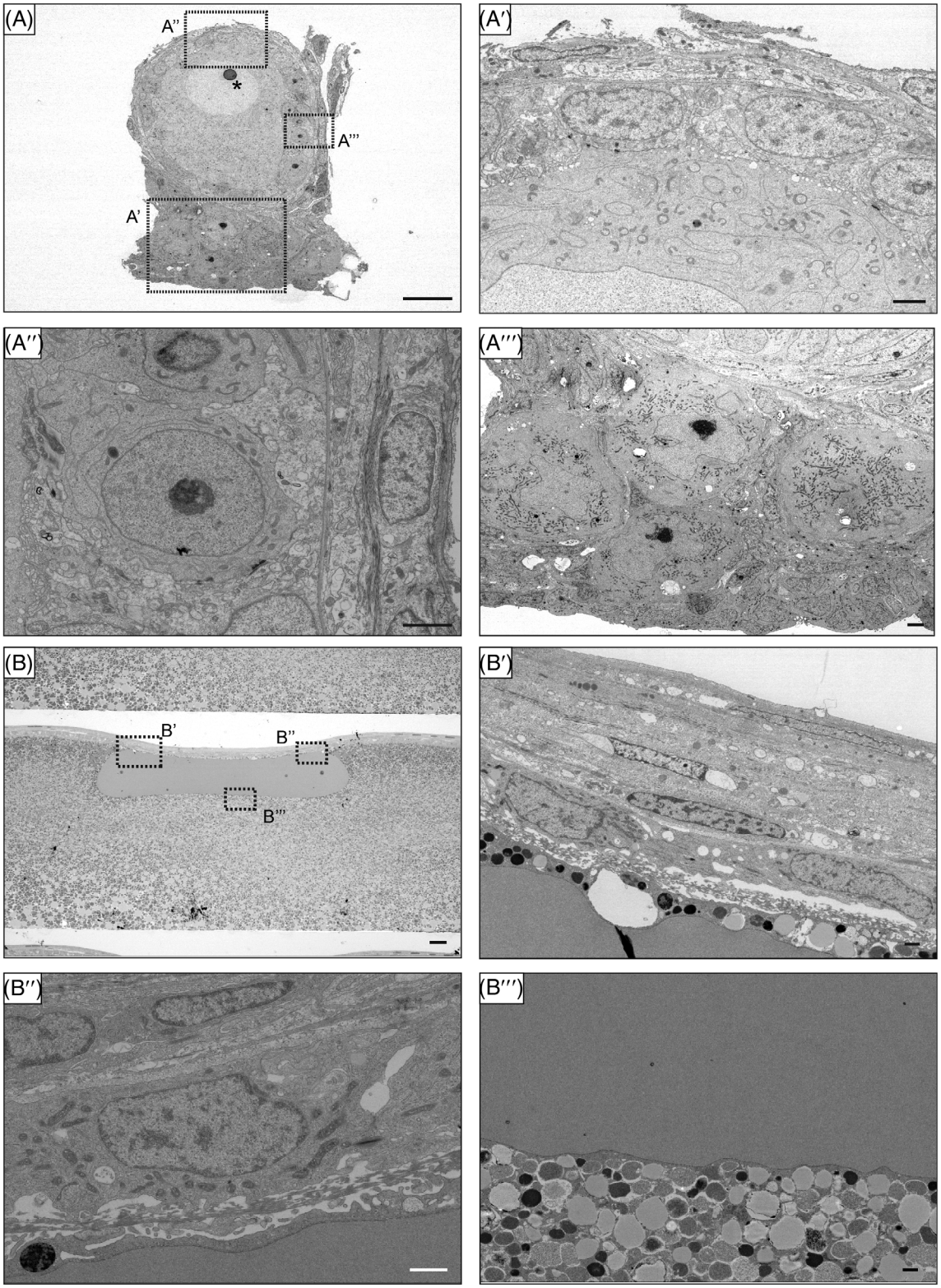

FIGURE 8 Raw data with no pseudo-coloring of subcellular architecture of the germinal bed II A/B. STEM of germinal bed and stage II follicle (A) and stage VIII follicle (B), re-analysis of data shown in Figure 3H. Non-annotated images shown in Figure 4. Squares indicate regions for higher magnifications. Scale bars: (A/B) = 20 μm. (A′)–(A‴) = 2 μm, (B′)–(B‴) = 1 μm.

cell layer. This double layer then becomes more pronounced during subsequent stages (Figure 9G). In older follicles (stages III–VII, Figure 9H), the inner basement membrane exhibits perforations (Figure 9H z140 higher magnification, right column). In contrast, the outer basement membrane instead appears to be deposited not only

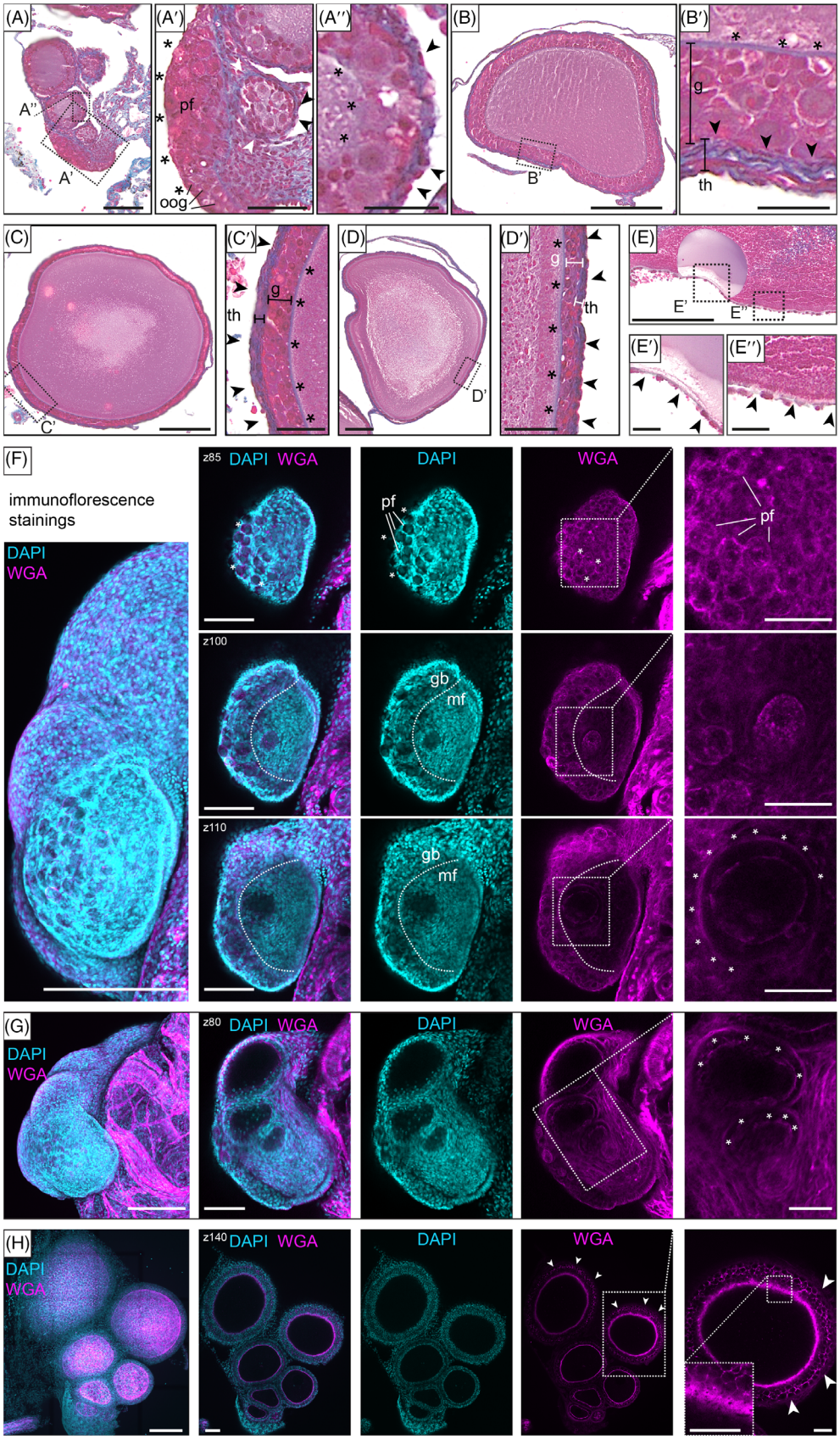

FIGURE 9 Legend on next page.

on the basal side of the cells, but also in-between the cells, enabling the definition of cell shapes (Figure 9H, WGA arrows). Thus, distinct basement membrane distribution patterns accompany follicle maturation, and include a characteristic pattern in the geminal bed and the acquisition of a double membrane around the granulosa cells as evidenced via both histology staining and WGA confocal imaging.

3 | DISCUSSION

In this study, we provide a comprehensive description of ovarian oocyte and follicle development in the brown anole (Figure 10A/B). Using brightfield and CT imaging as well as STEM, histological staining, and confocal microscopy, we define 10 consecutive stages of oogenesis and folliculogenesis. Our first 6 stages are combined into stage 1 of the staging system described for *A. pulchellus*,[9] and we defined one novel stage that precedes the 9 stages defined for *Tropidurus*[8] (Figure 10B Ia/Ib). To enable cross-species comparison, we designated these stages Ia and Ib instead of creating a novel competing staging system. Although ovarian follicles and follicle development have been described in the genus *Anolis* before,[9,35] our study contributes substantial new detail by providing a more detailed description dividing oogenesis into 10 stages based on granulosa cell morphology, yolk development, and follicle size changes in the brown anole ovary.

We found that in the brown anole ovary, the follicular epithelium undergoes stereotyped changes in cell type composition, and we hypothesize that each cell type has a different functional role in support of follicular development. We observed changes in the ratio of granulosa cell types as follicles mature, consistent with patterns observed in other lizards, and we identified the three known granulosa cell types: small cells, intermediate cells, and pyriform granulosa cells. While granulosa cells are known to play a critical role in the development of the mouse ovary,[18] we currently only have a limited understanding of the role of the different granulosa cell types in the brown anole ovary during oocyte development. Previous analyses of reptile ovaries posited different hypotheses regarding the function and origin of the different granulosa cell types.[7,10,36] However, no functional studies have tested these hypotheses to better understand the mechanism governing the consecutive reorganization of this highly dynamic structure. With our work, we lay the foundation for such stage-specific future functional analyses.

The exponential increase in follicle volume observed in our dataset is likely driven by the accumulation of yolk in the oocyte. We observe discernable stages of yolk deposition within the follicles but could not link the patterns to specific features within the granulosa cell layers. We observed that oogonia in the germinal bed do not stain positive for eosin, indicating a lack of cytoplasmic protein.[37] Later stages of follicles had eosin-positive cytoplasmic material, which is indicative of protein deposition. The protein required for yolk development, vitellogenin, has been reported in turtles to be transported through blood vessels and to be deposited into the oocyte.[38,39] Interestingly, we observed perforations of the basement membrane in vitellogenic follicles that could enable growth of the follicle but may also serve as sites of yolk transfer through the basement membrane. Further studies are required to understand the precise mechanism of yolk deposition in the brown anole oocyte.

We observe that a basement membrane is established in early follicles and that at later stages of follicular development, a double basement membrane is present. Basement membranes are assembled from laminin secreted by epithelial cells and are required to establish appropriate tissue architecture and structure.[40] In our data, we show that gaps develop in the basement membrane of mature, pre-ovulatory follicles. In mice, the embryonic basement membrane has been shown to be actively remodeled during implantation and gastrulation so that

FIGURE 9 Basement membrane deposition during follicle maturation (A)–(E). Trichrome staining of stage I–IX follicle cross sections. Square indicates higher magnifications. *Z* indicates the micron depth at which the optical section shown was collected. (A) Stage I–II, scale bar = 100 μm (A′) higher magnification of oogonia (oog, asterisks) and primordial follicles (pf, arrows), scale bar = 50 μm, (A″) stage II follicle, scale bar = 25 μm. (B) Stage V follicle, scale bar = 200 μm. (B′) Higher magnification illustrates basement membrane surrounding the follicle (arrows) and basement membrane within the theca cell layer (th) (asterisks), scale bar = 25 μm. (C) Stage VI follicle, scale bar = 200 μm. (C′) Double basement membrane around the granulosa cell layer (g) remains, scale bar = 50 μm. (D) Stage VIII follicle, scale bar = 200 μm. (D′) Double basement membrane around the granulosa cell layer remains, scale bar = 50 μm. (E) Stage IX follicle, scale bar = 200 μm. (E′/E″) Higher magnification of follicular epithelial cell layer, only one thin basement membrane detected, scale bar = 25 μm. (F)–(H) Immunofluorescence staining of follicle development. DAPI (cyan) and WGA (magenta) staining. Left maximum intensity projection, scale bar = 200 μm. Middle 3 columns individual z-sections, scale bar = 100 μm. Boxes indicate higher magnification in the right column, scale bar = 50 μm. (F) Germinal bed, z85 asterisks highlight germ cells, pf = primordial follicles. z100/z110 dashed lines indicate the border of the germinal bed (gb) to the left, maturing follicles (mf) to the right. z110 higher magnification asterisks indicate stage II. (G) Stage II–IV follicles. Higher magnification: asterisks highlight double basement membrane. (H) Stage III–V follicles. Arrows indicate outer basement membrane deposited pericellularly. Right: Higher magnification of perforations in inner basement membrane.

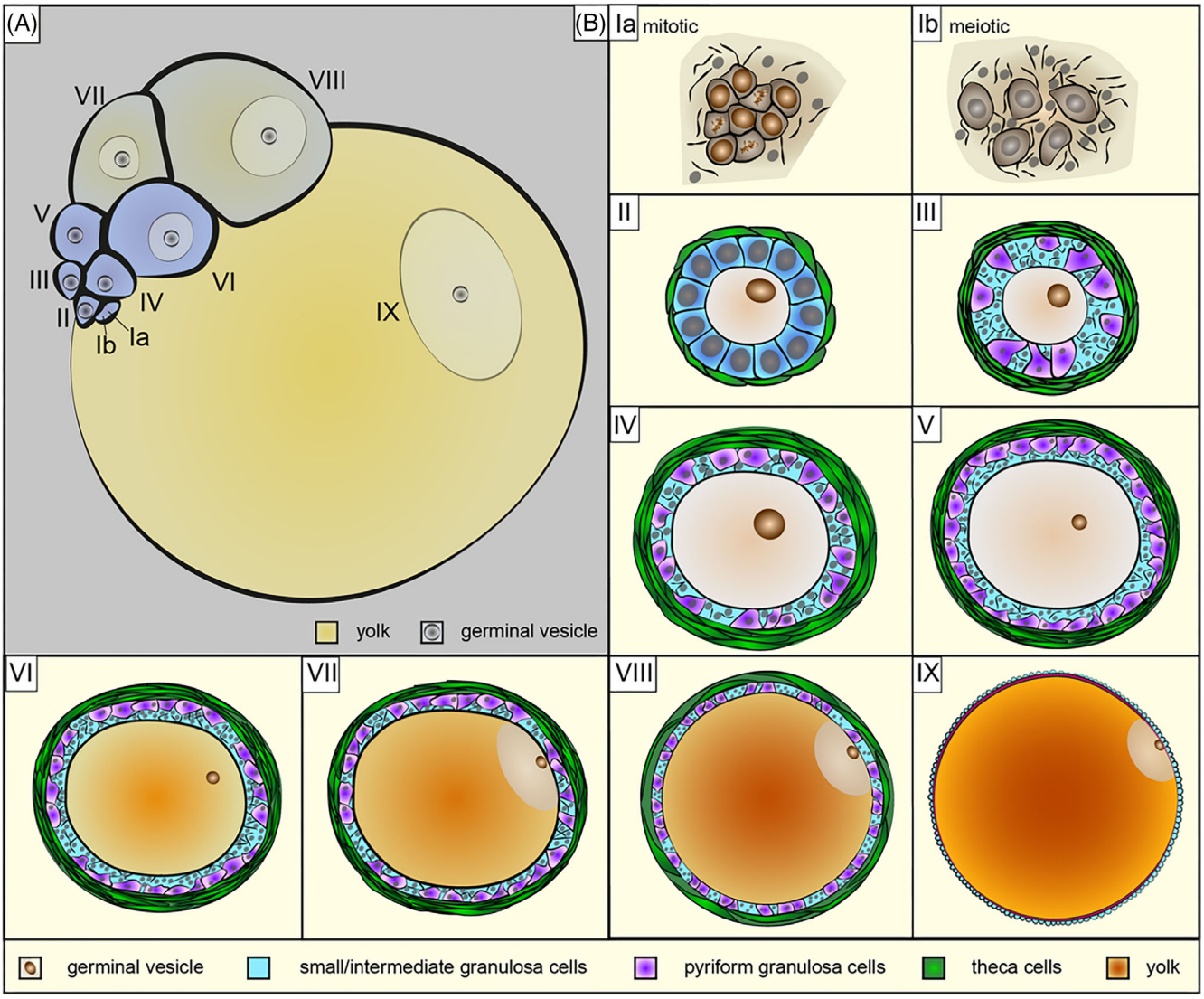

FIGURE 10 Schematic of follicle development in the brown anole. (A) Schematic drawing of a brown anole ovary. The follicles are annotated with the corresponding developmental stage (Ia-IX). (B) Schematic drawings of follicle developmental stages Ia-IX. Each schematic includes the main characteristics of each stage but is not scaled toward each other.

perforations appear and are distributed asymmetrically, contributing to anterior–posterior axis formation.[41,42] The perforations we observe in the brown anole basement membrane surrounding the oocyte could be part of an active remodeling process during oocyte maturation. These perforations could also serve to facilitate vitellogenin acquisition from the bloodstream, as discussed above. The double basement membrane is also remarkable. A dual membrane is characteristic of other organs, for instance, the glomerular basement membrane in the developing kidney. In this case, the dual membrane results from fusion of membranes secreted by epithelial and endothelial cells.[43] In our case, it is unclear exactly what the origin of the dual membrane is. Additional work on the development and function of the oocyte basement membrane would therefore be beneficial.

We identified a single germinal bed per ovary which is separated from the maturing follicles of the ovary. Mechanisms leading to oogenesis initiation, including how maturing follicles leave the germinal bed to begin maturation, are poorly understood. This movement and rearrangement of the basement membrane may be orchestrated by granulosa cells. However, we still need to gain a deeper understanding of the gene expression patterns of the cells that constitute the germinal bed as well as the early follicles to answer this question. Similarly, because other non-avian reptile species, such as lizards in the genera *Sceloporus* and *Basiliscus*,[6] can have multiple germinal beds per ovary and because clutch size is highly variable across reptiles, examining how the number of oogonial divisions per reproductive cycle correlates with clutch sizes

would be interesting and of evolutionary and developmental biology value.

Our study establishes that brown anole oogenesis occurs in a pattern conserved with other lizards. We present a staging table of follicle development that will lay the basis for functional and cross-clade comparative studies of oogenesis, further cementing the brown anole as a representative species of the genus *Anolis*. Through this precise staging system, the timing of genome editing may be more precisely defined, enabling reproducibility and identification of the optimal timepoint for genome modification. Understanding oogenesis in reptiles also has a broader potential to influence the field of Assisted Reproductive Technology. Identification of the factors that facilitate continuous germ cell production within the germinal bed across the adult life of a non-avian reptile may open novel avenues to counter infertility in mammals that have a finite number of oocytes.[44]

4 | METHODS

4.1 | Collection of females

All animal collection and procedures used in this study were approved by MD Anderson Cancer Center IACUC (#00002169), the University of Florida IACUC (#201408266) or the Loyola University Chicago IACUC (#3662). *A. sagrei* females were collected at the Houston Arboretum in summer 2021, Gainesville, FL, summer 2016–2017, and in Miami, FL, May 2023 according to state regulations. Females were euthanized according to one of the following protocols: In Houston, females were anesthetized with 1% Tricaine followed by 50% tricaine injection. In Gainesville, anoles were euthanized using Euthasol, fixed using 10% formalin. In Miami, females were placed in a cooling box with an ice pack to slow down metabolism for anesthesia and then euthanized through decapitation. In Houston, anoles were anesthetized by 1% Tricaine dosed by weight and then euthanized by a 50% tricaine injection dosed by weight (Conroy 2009).

4.2 | MicroCT

A. sagrei were fixed using 10% formalin and stored in 70% ethanol. Then, specimens were stained with 1.75% aqueous Lugol's iodine (Gignac, Kley et al. 2016) and their whole body was visualized with x-ray computed tomography. All samples were scanned on GE V|Tome|X M 240 system at Nanoscale Research Facility at the University of Florida. Source and detector settings are listed in Table 1. Tomograms were generated using Reconstructor software v.16.0.11592 (Carl Zeiss Microscopy, GmbH), and segmentation was done using 3D-slicer.[45] All animal collection and procedures for these methods were approved by the University of Florida IACUC.

4.3 | Histology

Samples were previously fixed and stored in 70% ethanol as described above. Samples were paraffin processed (Milestone, Pathos Delta Microwave Tissue Processor) and subsequently embedded in paraffin wax (CancerDiagnostics, PureAffin® R56). Samples were then sectioned at a thickness of 5 μm on a microtome (Leica RM2255). H&E staining was performed using an automatic stainer (DP360, Dakewe [Shenzen] Medical Equipment Co.) with ST Infinity H&E Reagents (Leica Biosystems Cat. 3801698). Slides were mounted with Cytoseal 60 mounting media (VWR, 48212-187).

4.4 | Electron microscopy

Samples were prepared for electron microscopy as previously described.[30] Sections were cut at 80 nm with a Diatome diamond knife and stained with 6 min each of 4% uranyl acetate in 70% methanol and Sato's triple lead stain before imaging in a Zeiss Merlin SEM with aSTEM detector at 26 kV and 700 pA.

4.5 | Confocal imaging

Ovaries were incubated in DAPI and Wheat Germ Agglutinin (AF-594) and imaged on a Zeiss LSM800 or Zeiss LSM900. Optical sections for whole-mount fluorescent staining samples were collected at 5 μm intervals. Tile scans were collected with 15% overlap.

4.6 | Computational analysis

Brightfield images were rendered using the Helicon Software. All quantitative analyses were carried out using FIJI (Schindelin et al., 2012).

4.7 | Quantitative analysis

4.7.1 | Volumetric analysis of CT data

We reanalyzed the datasets published in Kircher and McCowen et al. (2024) to represent anoles 1 and 2 (Morphosource

ID: 000590186, 000608703). Anole 3 has been uploaded to Morphosource (ID: 000702213). To compare the volume of each follicle on the ovary, we digitally segmented in 3D slicer[45] each follicle and determined the volume from the digital 3D dataset. We measured the snout-vent-length (SVL) of the lizard and divided the ovarian follicle volume by the SVL of the lizard to correct for body size. We log-transformed the body-size-corrected follicle volume and multiplied that volume by −1. We also ranked each follicle by the volume of the follicle compared to the others on the ovary. The smallest follicle is ranked number 1 and each follicle with increasing volume has a progressively higher rank. We graphed the body-size-corrected volume against follicle rank and added error bars representing standard deviation from the mean value of each follicle rank using R (version 4.5.0) in R Studio (2025.05.0 + 496). We also analyzed the change in follicular volume across each individual ovary sampled in our dataset using a linear regression model in R (version 4.5.0) in R Studio (2025.05.0 + 496).

4.7.2 | Percentage of large cells

For each follicle, the cross section of the largest diameter was chosen. All cells within the granulosa cell layer were counted. The number of large cells (including intermediate and pyriform cells) was divided by the total number of cells. The percentage was plotted using R (version 4.5.0) in R Studio (2025.05.0 + 496). We fit a linear regression model using the geom_smooth function in ggplot2.

4.7.3 | Follicular epithelium width

Linear measurements of the follicular epithelium were taken for each follicle again at the cross section that showed the largest diameter for the respective follicle.

4.7.4 | Width

Measurements were collected in three places around the circumference of the follicle. The average of these three measurements was plotted against the follicle stage using R (version 4.5.0) in R Studio (2025.05.0 + 496). A generalized additive model was fitted using the geom_smooth function in ggplot2.

4.7.5 | Plot profiles

Plot profiles were drawn across the width of the oocyte (Figure 4A–C). Plot profiles were drawn to avoid the nucleus and any sectioning artifacts (tears, wrinkles, etc., Figure 4A–C). Line width of the plot profile was 10 μM for pv follicles and 100 μM for ev, vitellogenic, and mature vitellogenic follicles. Higher mean gray value indicates higher density while lower mean gray value indicates lower density.

ACKNOWLEDGMENTS

The authors thank all members of the Trainor, Behringer & Williams labs for critical feedback. We thank Edward Stanley and Martin Cohn at the University of Florida for support generating the CT data. Research in the Trainor lab is funded by the Stowers Institute for Medical Research (1008). The Behringer lab is supported by NIH grants 5R01HD113569 and HD30284 and the Ben F. Love Endowment to Richard R. Behringer. Bonnie K. Kircher was supported by National Science Foundation (NSF) Postdoctoral Research Fellowship in Biology (PRFB), Division of Biological Infrastructure (DBI) 2209150 and NIH T32HD098068. MicroCT scanning was supported by a NSF Graduate Research Fellowship awarded to Bonnie K. Kircher. Veterinary services were supported by NIH grant CA16672. The Sanger lab is funded through the USA National Science Foundation (#1942250). A.W. is the recipient of an independent postdoctoral research fellowship of All Souls College, University of Oxford, and received a travel grant from the Cambridge Philosophical Society. A.W. and F.H. are supported by the Newton Trust, the European Research Council (695669) and the Engineering and Physical Sciences Research Council (EP/Y032756/1). NAS is supported by a K99/R00 Pathway to Independence award from the National Institute of Child Health and Human Development (HD114881).

CONFLICT OF INTEREST STATEMENT

The authors declare no conflict of interest.

DATA AVAILABILITY STATEMENT

Original data underlying this manuscript can be accessed upon publication at the Stowers Original Data Repository at https://www.stowers.org/research/publications/libpb-2591 CT data for anoles 1 and 2 reanalyzed from Kircher and McCowen et al. (2024). All scans have been uploaded to Morphosource (Anole 1 Morphosource ID: 000590186, Anole 2 Morphosource ID: 000608703, Anole 3 Morphosource ID: 000702213).

ORCID

Antonia Weberling https://orcid.org/0000-0001-8282-5695

Paul A. Trainor https://orcid.org/0000-0003-2774-3624

REFERENCES

1. Beaumont HM, Mandl AM. A quantitative and cytological study of oogonia and oocytes in the foetal and neonatal rat. *Proc R Soc Lond B Biol Sci*. 1962;155(961):557-579.
2. Dubois R, Croisille Y. Germ-cell line and sexual differentiation in birds. *Phil Trans R Soc London B, Biol Sci*. 1970;259(828):73-90.
3. Guraya SS, Varma SK. Morphology of ovarian changes during the reproductive cycle of the house lizard, *Hemidactylus flaviviridis*. *Acta Morphol Neerl Scand*. 1976;14(2):165-192.
4. Guraya SS. *Ovarian Follicles in Reptiles and Birds*. Vol 24. Springer Science & Business Media; 2013.
5. Nie H, Xu Y, Zhang Y, et al. The effects of endogenous FSH and its receptor on oogenesis and folliculogenesis in female *Alligator sinensis*. *BMC Zool*. 2023;8(1):8.
6. Jones RE, Swain T, Guillette JLJ, Fitzgerald KT. The comparative anatomy of lizard ovaries, with emphasis on the number of germinal beds. *J Herpetol*. 1982;16:240-252.
7. Klosterman LL. The ultrastructure of germinal beds in the ovary of *Gerrhonotus coeruleus* (Reptilia: Anguidae). *J Morphol*. 1983;178(3):247-265.
8. da Silva D, Cassel M, Mehanna M, Ferreira A, Dolder MAH. Follicular development and reproductive characteristics in four species of Brazilian *Tropidurus* lizards. *Zoolog Sci*. 2018;35(6):553-563.
9. Ortiz E, Morales MH. Development and function of the female reproductive tract of the tropical lizard, *Anolis pulchellus*. *Physiol Zool*. 1974;47(4):207-217.
10. Neaves WB. Intercellular bridges between follicle cells and oocyte in the lizard, *Anolis carolinensis*. *Anat Rec*. 1971;170(3):285-301.
11. Lozano A, Ramírez-Bautista A, Uribe MC. Oogenesis and ovarian histology in two populations of the viviparous lizard *Sceloporus grammicus* (Squamata: Phrynosomatidae) from the central Mexican plateau. *J Morphol*. 2014;275(8):949-960. doi:10.1002/jmor.20275
12. Aldokhi OA, Alwasel S, Harrath AH. Ultrastructural and histochemical study of previtellogenic oogenesis in the desert lizard *Scincus mitranus* (Squamata, Sauropsida). *J Morphol*. 2019;280(3):381-394. doi:10.1002/jmor.20950
13. Uribe M, Omana MEM, Quintero JG, Guillette LJ Jr. Seasonal variation in ovarian histology of the viviparous lizard *Sceloporus torquatus torquatus*. *J Morphol*. 1995;226(1):103-119. doi:10.1002/jmor.1052260107
14. Moodley GK, van Wyk JH. Folliculogenesis and ovarian histology of the oviparous gecko, *Hemidactylus mabouia* (Sauria: Gekkonidae). *Afr J Herpetol*. 2007;56(2):115-135.
15. Vieira S, de Pérez GR, Ramírez-Pinilla MP. Ultrastructure of the ovarian follicles in the placentotrophic Andean lizard of the genus *Mabuya* (Squamata: Scincidae). *J Morphol*. 2010;271(6):738-749. doi:10.1002/jmor.10830
16. Varma SK. Morphology of ovarian changes in the garden lizard, *Calotes versicolor*. *J Morphol*. 1970;131(2):195-209.
17. Dekel N. Interaction between the oocyte and the granulosa cells in the preovulatory follicle. *Endocrinology and Physiology of Reproduction*. Springer; 1987:197-209.
18. Nilsson E, Skinner MK. Cellular interactions that control primordial follicle development and folliculogenesis. *J Soc Gynecol Investig*. 2001;8(Suppl 1):S17-S20.
19. Ramírez-Pinilla MP, de Pérez GR, Alvarado-Ramírez C. Oogenesis and the ovarian cycle. *Reproductive Biology and Phylogeny of Lizards and Tuatara*. CRC Press; 2015:213-252.
20. Jones RE, Tokarz RR, LaGreek FT. Endocrine control of clutch size in reptiles. V. FSH-induced follicular formation and growth in immature ovaries of *Anolis carolinensis*. *Gen Comp Endocrinol*. 1975;26(3):354-367.
21. Muñoz MM, Frishkoff LO, Pruett J, Mahler DL. Evolution of a model system: new insights from the study of *Anolis* lizards. *Annu Rev Ecol Evol Syst*. 2023;54:475-503.
22. Malkmus J, Ramos Martins L, Jhanwar S, et al. Spatial regulation by multiple Gremlin1 enhancers provides digit development with cis-regulatory robustness and evolutionary plasticity. *Nat Commun*. 2021;12(1):5557.
23. Gredler ML, Larkins CE, Leal F, et al. Evolution of external genitalia: insights from reptilian development. *Sex Dev*. 2014;8:311-326. doi:10.1159/000365771
24. Marchini M, Keller G, Khan N, et al. Sonic hedgehog and fibroblast growth factor 8 regulate the evolution of amniote facial proportions. *Commun Biol*. 2025;8(1):84.
25. Griffing AH, Gamble T, Cohn MJ, Sanger TJ. Convergent developmental patterns underlie the repeated evolution of adhesive toe pads among lizards. *Biol J Linn Soc*. 2022;135(3):518-532.
26. Geneva AJ, Park S, Bock DG, et al. Chromosome-scale genome assembly of the brown anole (*Anolis sagrei*), an emerging model species. *Commun Biol*. 2022;5(1):1-13.
27. Rasys AM, Park S, Ball RE, Alcala AJ, Lauderdale JD, Menke DB. CRISPR-Cas9 gene editing in lizards through microinjection of unfertilized oocytes. *Cell Rep*. 2019;28(9):2288-2292.e3. doi:10.1016/j.celrep.2019.07.089
28. Samudra SP, Park S, Esser EA, et al. A new cell culture resource for investigations of reptilian gene function. *Development*. 2024;151(22):dev204275.
29. Kircher BK, Stanley EL, Behringer RR. Anatomy of the female reproductive tract organs of the brown anole (*Anolis sagrei*). *Anat Rec*. 2023;307:395-413.
30. Weberling A, Shylo NA, Kircher BK, et al. Pre-oviposition development of the brown anole (*Anolis sagrei*). *Dev Dyn*. 2025:1-23.
31. Sanger TJ, Losos JB, Gibson-Brown JJ. A developmental staging series for the lizard genus *Anolis*: a new system for the integration of evolution, development, and ecology. *J Morphol*. 2008;269(2):129-137. doi:10.1002/jmor.10563
32. Crews D. The annotated anole: studies on control of lizard reproduction: anoline lizards make excellent experimental animals for analyzing reproduction at the physiological, behavioral, and species levels. *Am Sci*. 1977;65(4):428-434.
33. Crews D. Interrelationships among ecological, behavioral, and neuroendocrine processes in the reproductive cycle of *Anolis carolinensis* and other reptiles. *Adv Stud Behav*. 1980;11:1-74.
34. Grier HJ, Uribe MC, Lo Nostro FL, Mims SD, Parenti LR. Conserved form and function of the germinal epithelium through 500 million years of vertebrate evolution. *J Morphol*. 2016;277(8):1014-1044.
35. Laughran LJ, Larsen JH Jr, Schroeder PC. Ultrastructure of developing ovarian follicles and ovulation in the lizard *Anolis carolinensis* (Reptilia). *Zoomorphology*. 1981;98(3):191-208.

36. Filosa S, Taddei C, Andreuccetti P. The differentiation and proliferation of follicle cells during oocyte growth in *Lacerta sicula*. *Development*. 1979;54(1):5-15.
37. Nuovo GJ. *In Situ Molecular Pathology and co-Expression Analyses*. Academic Press; 2020.
38. Ho S-M, Kleis S, McPherson R, Heisermann G, Callard I. Regulation of vitellogenesis in reptiles. *Herpetologica*. 1982;38:40-50.
39. Gapp D, Ho S, Callard I. Plasma levels of vitellogenin in *Chrysemys picta* during the annual gonadal cycle: measurement by specific radioimmunoassay. *Endocrinology*. 1979;104(3):784-790.
40. Ecay TW, Valentich JD. Basal lamina formation by epithelial cell lines correlates with laminin a chain synthesis and secretion. *Exp Cell Res*. 1992;203(1):32-38.
41. Chen D-Y, Claussen NH, Titus S, et al. Basement membrane perforations guide anterior–posterior axis formation. *Nat Commun*. 2025;16(1):6763.
42. Kyprianou C, Christodoulou N, Hamilton RS, et al. Basement membrane remodelling regulates mouse embryogenesis. *Nature*. 2020;582(7811):253-258.
43. Abrahamson D. Structure and development of the glomerular capillary wall and basement membrane. *Am J Physiol Renal Physiol*. 1987;253(5):F783-F794.
44. Hutchinson AM, Weberling A, Endo Y, Bargaje R. Outside the box: comparative stem cell insights for fertility biotechnology and conservation. *F&S Rep*. 2025;6:38-44.
45. Fedorov A, Beichel R, Kalpathy-Cramer J, et al. 3D slicer as an image computing platform for the quantitative imaging network. *Magn Reson Imaging*. 2012;30(9):1323-1341.

How to cite this article: Kircher BK, Weberling A, Vance EJ, et al. Oogenesis and germinal bed morphology of the brown anole (*A. sagrei*). *Developmental Dynamics*. 2026;1-22. doi:10.1002/dvdy.70112